is no consensus so far on the levels of antioxidant enzymes in tumor cells; their expression increases in some case, and decreases in others [14–16].

Although the effects of ROS on tumor metastasis are not yet fully understood, antioxidant enzymes are sometimes used to suppress or reduce tumor metastasis *in vivo*. Catalase and/or superoxide dismutase (SOD) are used to prevent experimental tumor metastasis to the lung or liver [17, 18]. These enzymes, however, can detoxify ROS (superoxide anion for SOD, and H_2O_2 for catalase) only at local sites reached by the enzymes following their administration. SOD (CuZn-, recombinant human), with a molecular weight of 32 kDa, undergoes rapid glomerular filtration and is quickly cleared from the circulation [19]. Catalase (bovine liver) also disappears from the circulation, but its major clearance route is uptake by hepatocyte [20]. In previous studies, we demonstrated that the tissue distribution characteristics of protein drugs can be controlled by chemical modification: alteration of the electric charge, glycosylation, and conjugation of inert polymers such as poly(ethylene glycol) [21, 22]. Catalase and SOD have also been used for such modifications [23, 24]. Targeting of these antioxidant enzymes to liver nonparenchymal cells or the kidney increases their potential to prevent ROS-mediated tissue injuries [20, 23–26]. These findings clearly indicate that targeted delivery of these enzymes to sites where ROS are generated is very important for obtaining their maximal biological effects. Prolongation of the plasma half-life of catalase by attachment of poly(ethylene glycol) successfully improved the anti-metastatic effect of the enzyme in an experimental pulmonary metastasis model [27].

The purpose of this study is to examine the effects of catalase and its various derivatives with diverse pharmacokinetic characteristics on hepatic metastasis of colon carcinoma cells. Firstly, tissue distribution of the tumor cells is studied following intraportal injection of ^{111}In-labeled cells. Then, the effect of each treatment on liver metastasis is examined by measuring the number of metastatic colonies in the liver as well as the tissue weight of the liver. Finally, the MMP activity in tumor bearing liver is examined by *in situ* gelatin zymographic assay and by a gelatinase/collagenase assay. Here we present results showing that a single, bolus intravenous injection of catalase greatly reduces the number of metastatic colonies in the liver and galactosylation of the antioxidant enzyme greatly increases this suppressant effect of catalase on hepatic metastasis of colon carcinoma cells.

Materials and methods

Animals

BALB/c (four weeks old, male), CDF_1 (six weeks old, male) and ddY (six weeks old, male) mice were purchased from the Shizuoka Agricultural Cooperative Association for Laboratory Animals (Shizuoka, Japan). Animals were maintained under conventional housing conditions. All animal experiments were conducted in accordance with the principles and procedures outlined in the National Institute of Health Guide for the Care and Use of Laboratory Animals. The protocols for animal experiments were approved by the Animal Experimentation Committee of Graduate School of Pharmaceutical Sciences of Kyoto University.

Chemicals

Bovine liver catalase (35 000 units/mg) was purchased from Sigma Chemical (St. Louis, Missouri). ^{111}Indium chloride ($[^{111}In]Cl_3$) was supplied by Nihon Medi-Physics (Takarazuka, Japan). All other chemicals were of the highest grade available.

Synthesis of catalase derivatives

Three types of catalase derivatives, galactosylated (Gal-CAT), succinylated (Suc-CAT), and mannosylated catalase (Man-CAT), were synthesized as reported previously [24]. Inactivated catalase was prepared according to the method of Miyahara and Samejima [28]. The enzymatic activity of catalase derivatives was measured by monitoring their ability to degrade hydrogen peroxide.

Tumor cells

Colon 26 tumor cells, obtained from Dr Takao Yamori of Cancer Chemotherapeutic Center of Cancer Institute (Tokyo, Japan), were prepared as previously reported [27]. For tissue distribution experiments on tumor cells in mice, colon 26 cells were radiolabeled using ^{111}In-oxine, according to the method of Thakur et al. [29]. Briefly, 140 μl $^{111}InCl_3$ solution was added to 2 ml distilled water and 200 μl acetate buffer (0.3 M, pH 5.0). To ethanol anhydride was added 100 μg oxine and, then, the solution was added to the ^{111}Indium solution. The mixture was extracted in an equal volume of chloroform, which was then evaporated to dryness. This pellet was dissolved in 100 μl ethanol anhydride and 500 μl saline was added. A suspension of colon 26 tumor cells (10^7 cells/ml) in RPMI 1640 containing 10 % fetal bovine serum was incubated in the radioactive complex solution, then washed several times with Hanks' balanced salt solution (HBSS).

Tissue distribution of colon 26 tumor cells in mice

Under ether anesthesia, a midline incision was made in the abdomen of mice and the portal vein was exposed. ^{111}In-labeled colon 26 cells (1×10^5 cells/100 μl HBSS) were injected into the portal vein and the incision was closed with metal clips. At 1, 8 and 24 h after injection, blood was collected from the vena cava under ether anesthesia, and the mice were sacrificed. The liver, kidney, spleen, lung, and heart were removed and rinsed with saline. Radioactivity in blood and tissue samples was counted with a well-type NaI-scintillation counter ARC-500 (Aloka, Tokyo, Japan). Results were expressed as the percentage of the injected dose of radioactivity.

Experimental hepatic metastasis and treatment with catalase derivatives

CDF_1 or BALB/c mice were anaesthetized by intraperitoneal injection of pentobarbital sodium (50 mg/kg). A midline abdominal incision was made to expose the portal vein. Colon 26 tumor cells (1×10^5 cells/0.1 ml HBSS) was injected into the portal vein of mice using a syringe with a 29 G-needle. Then the opening was sutured and mice were allowed to recover. Catalase or its derivative was injected through the tail vein at a dose of 35 000 catalase units/kg (about 1 mg/kg for unmodified catalase) 3 days after tumor injection.

Number of metastatic colonies and liver weight

Fourteen days after tumor injection, mice were killed and the number of the tumor colonies on the surface of the liver was counted. The wet tissue weight of the liver was also measured.

In situ *zymography*

At 18 h after injection of catalase or Gal-CAT, mice were killed and the liver was excised. The liver was embedded in OTC compound (MILES Inc., Elkhart, Indiana) and cut into 8 μm-frozen sections. Serial cryosections were put onto gelatin-coated film (MMP *in situ* Zymo-Film; Wako Chemical, Osaka, Japan) and incubated at 37 °C for 24 h. Then gelatin left undegraded on the film was stained with Biebrich Scarlet Stain Solution (Wako Chemical, Osaka, Japan). Gelatin-coated film containing 1,10-phenanthroline (MMP-PT *in situ* Zymo-Film; Wako Chemical, Osaka, Japan), a gelatinase inhibitor, was also used to check whether the gelatinolysis is mediated by metalloenzymes including MMPs within the sections.

Measurement of MMP activity in tumor-bearing liver

Three or eight days after tumor injection into the portal vein, saline, catalase or Gal-CAT was injected into mice as above. At 18 h after injection, mice were killed and the liver was excised, weighed and homogenized with a lysis buffer (0.05% Triton X-100, 0.1 M Tris, pH 7.8) using a handy homogenizer. MMP activity of the supernatant was assayed using a gelatinase/collagenase assay kit (EnzChek, Molecular Probes, Eugene, Oregon). In addition, the MMP activity in the tumor-bearing liver was also measured by gelatin zymography. The supernatant of liver homogenates was electrophoresed on a 7.5% polyacrylamide gel containing 0.1% gelatin. After electrophoresis, the gel was washed twice with 2.5% Triton X-100 for 30 min at room temperature to remove sodium dodecyl sulfate. The gel was subsequently washed with 50 mM Tris (pH 8.0) for 30 min at room temperature. Then, the gel was incubated in a reaction buffer (50 mM Tris (pH 8.0), 0.5 mM $CaCl_2$, and 10^{-6} M $ZnCl_2$) for 24 h at 37 °C, stained with Coomasie brilliant blue R-250 and destained with methanol/acetic acid/water (5:7:88). Proteolysis was detected as white bands in a dark field. Relative gelatinolytic activity was evaluated by computerized densitometry (ATTO, Tokyo, Japan). To confirm the involvement of MMPs in the gelatinolysis, (2R)-[(4-biphenylylsulfonyl)amino]-N-hydroxy-3-phenylpropionamide (Calbiochem), a specific MMP-2/MMP-9 inhibitor, was added to the polyacrylamide gel. The molecular weights of gelatinases detected were estimated by using a set of marker proteins (full range rainbow marker, Amersham, Little Chalfont, UK).

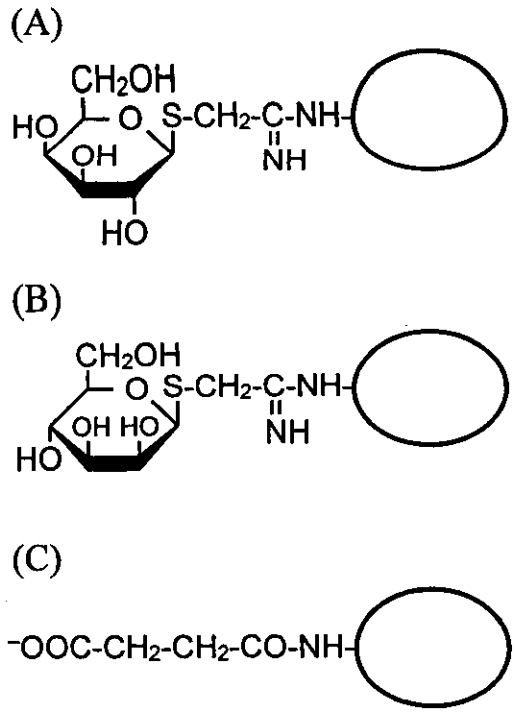

Figure 1. Chemical structures of catalase derivatives. (A) galactosylated catalase (Gal-CAT), (B) mannosylated catalase (Man-CAT), and (C) succinylated catalase (Suc-CAT). Each oval represents bovine liver catalase.

Statistical analysis

Differences were statistically evaluated by one-way ANOVA followed by the Student–Newmann–Keuls multiple comparison test.

Results

Catalase derivatives

The chemical structures of the catalase derivatives are shown in Figure 1. As reported in previous paper from our laboratory [24], the enzymatic activity of the catalase derivatives was preserved to a sufficient degree: each derivative exhibited 86% (Suc-CAT), 90% (Gal-CAT), and 97% (Man-CAT) of the original enzymatic activity to degrade H_2O_2.

Tissue distribution of colon 26 tumor cells

Figure 2 shows the radioactivity in tissue samples of mice injected with ^{111}In-colon 26 tumor cells via the portal vein. After intraportal injection, approximately 50 to 60% of the radioactivity was recovered in the liver at all time points examined. Radioactivity in the blood gradually decreased

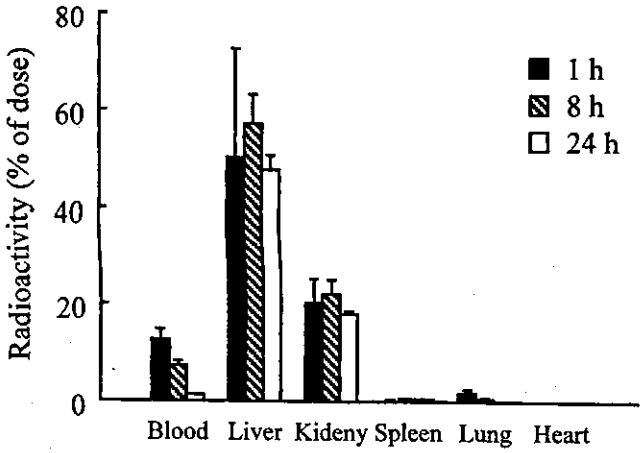

Figure 2. Tissue distribution of radioactivity in mice following intraportal injection of ^{111}In-colon 26 tumor cells. Results are expressed as the mean + SD of three mice.

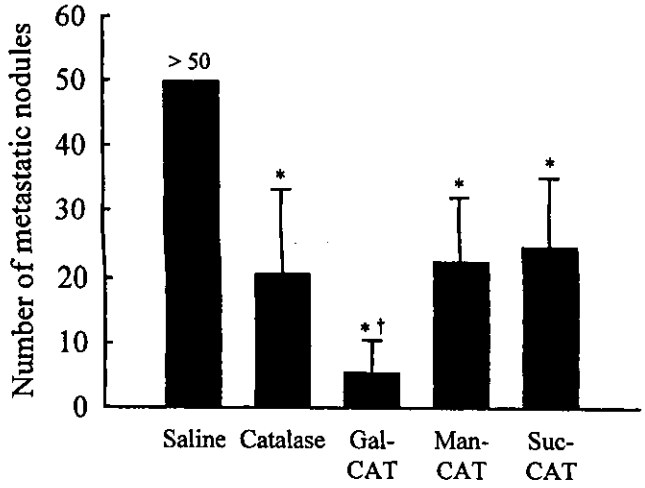

Figure 3. Number of metastatic colonies of colon 26 tumor cells on the liver surface of mice injected with saline (vehicle) or catalase derivative (35 000 units/kg). Mice were sacrificed at 14 days after tumor injection and the number of the colonies counted. Results are expressed as the mean + SD of at least 7 mice.
*A statistically significant difference compared with the saline group ($P < 0.001$); †a statistically significant difference compared with the catalase group ($P < 0.001$).

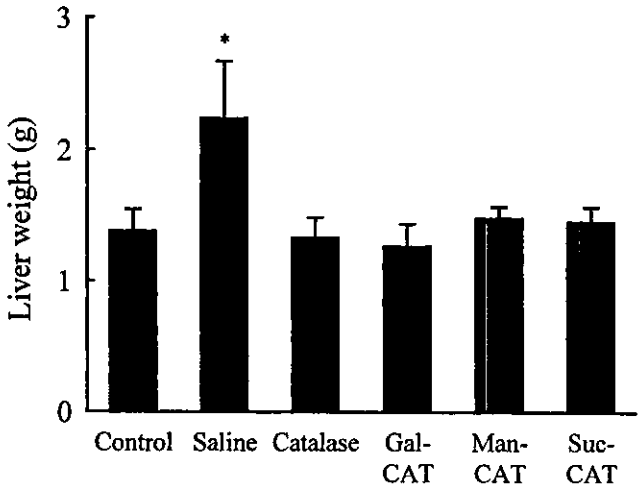

Figure 4. Weight of the liver of mice injected with colon 26 tumor cells followed by an injection of saline (vehicle) or catalase derivative (35 000 units/kg). Mice were sacrificed at 14 days after tumor injection and the liver weighed. Results are expressed as the mean + SD of at least 7 mice.
*A statistically significant difference compared with the saline group ($P < 0.001$).

with time. The amount of radioactivity accumulating in the kidney was about 20% of the dose at all time points, but less radioactivity was detected in the lung, spleen and heart. About 10% of the injected radioactivity was excreted into urine within 1 h following injection (data not shown), suggesting tumor cell lysis in the circulation or within tissues. The tissue distribution profile of the radioactivity following the intraportal injection of ^{111}In-colon 26 cells was different from that obtained following intravenous injection, with greater uptake by the lung and less uptake by the liver [27]. These results suggest that the tumor cells are mainly trapped in the liver when injected intraportally, probably due to the fact that the liver is the first-pass organ following intraportal injection.

Hepatic metastasis and its inhibition by catalase derivatives

When colon 26 tumor cells were injected into the portal vein, metastatic colonies were detected in the liver. The number of the colonies was greater than 50 at 2 weeks after the injection of 1×10^5 cells (Figure 3). In addition, the weight of the liver of mice injected with colon 26 cells was significantly ($P < 0.001$) greater than that of control mice (Figure 4).

An intravenous injection of catalase reduced the number of metastatic colonies in the liver (Figure 3). The administration of either Suc-CAT or Man-CAT gave similar numbers of the colonies to that obtained with catalase. The number of colonies in mice treated with catalase, Suc-CAT or Man-CAT was significantly smaller than that in the saline-treatment group ($P < 0.001$). Gal-CAT exhibited a greater inhibitory effect on the formation of colonies in the liver than the other catalase derivatives. The number of colonies was significantly smaller than under any of the other conditions examined ($P < 0.001$). The weight of the liver in mice injected with catalase or its derivative was comparable with that of control mice (Figure 4), because the colonies in the treated mice were much smaller than those in the saline-treated mice. The administration of either BSA or inactivated catalase had no significant effects on the hepatic metastasis (data not shown). These results indicate that the inhibitory effects of catalase derivatives on tumor metastasis are due to the catalase activity involved in the detoxification of H_2O_2.

MMP activity in colon 26 tumor cell-bearing mouse liver

A little gelatinolytic activity was seen in sections of normal mouse liver (Figure 5A). On the other hand, the liver sections from mice receiving colon 26 cells and treated with saline extensively degraded gelatin on the film (Figure 5B). The gelatin degradation by the tissue sections was greatly blocked by the presence of 1,10-phenanthroline, an inhibitor of metalloenzymes such as MMPs (Figure 5C), suggesting enzymatic degradation of gelatin. Liver sections from tumor-bearing mice receiving catalase (Figures 5D and E) or Gal-CAT (Figures 5F and G) showed reduced gelatin

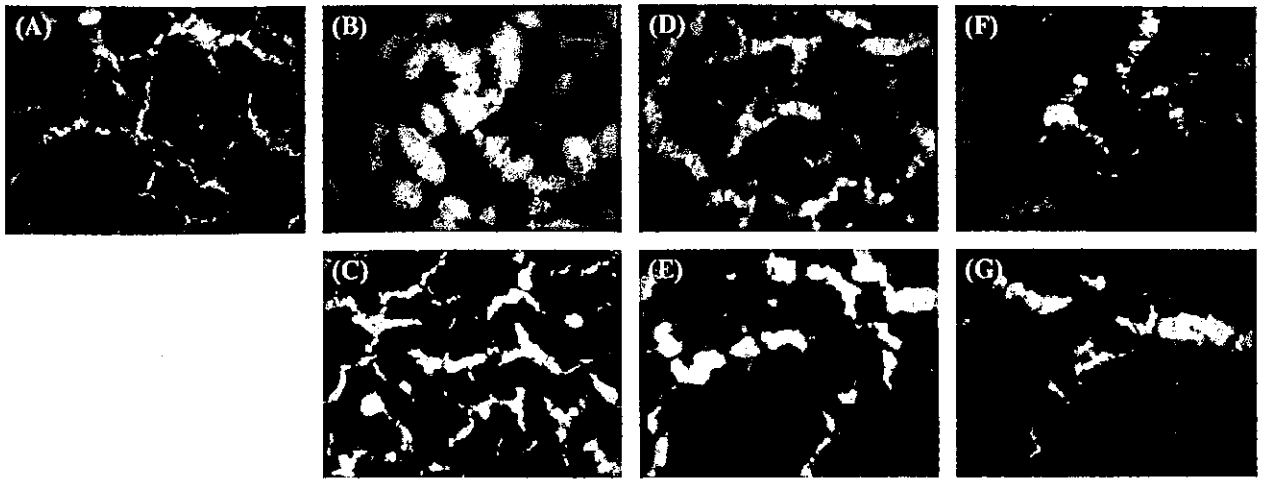

Figure 5. In situ gelatin zymography from mouse liver of (A) untreated mice, and of mice receiving intraportal injection of 1×10^5 colon 26 tumor cells followed by intravenous injection of saline (B, C), catalase (D, E) or Gal-CAT (F, G). Bottom images (C, E, G) were ones with gelatin-film containing a metalloenzyme inhibitor, 1,10-phenanthroline. Gelatinolytic activity is detected as yellowish brighter areas in the red-colored gelatin layer.

degradation, and the inhibitory effect of Gal-CAT was prominent. These results suggest that the presence of metastatic colon 26 tumor cells increases the gelatinolytic activity of the tumor-bearing liver tissues, and Gal-CAT efficiently prevent the increase.

Hepatic MMP activity

Figure 6A shows total MMP activity in the liver of mice receiving intraportal injection of 1×10^5 colon 26 tumor cells. Catalase or Gal-CAT was injected into mice at three or eight days after tumor inoculation. A detectable amount of MMP activity was found in the liver of untreated mice. Injection of tumor cells significantly increased the MMP activity of the liver. An intravenous injection of catalase somewhat reduced MMP activity of the liver. Furthermore, an injection of Gal-CAT at day 8 significantly reduced the gelatinolytic activity of the liver homogenates containing metastatic tumors ($P < 0.05$).

Figure 6B shows the gelatin zymographic analysis of the liver homogenates from tumor-bearing mice. No detectable bands were found in the liver homogenates of control mice (lane 1). On the other hand, a prominent band was seen in the homogenates of the tumor-bearing mice, which were treated with saline at 8 days after tumor inoculation (lanes 2, 3). This band was completely disappeared by the addition of the inhibitor of MMP-2 and -9, (2R)-[(4-biphenylylsulfonyl)amino]-N-hydroxy-3-phenylpropionamide, in the gel. In addition, the molecular markers indicated that the band observed in the saline-treated group corresponded to MMP-9. A slight activity of MMP-2 was also detected in this analysis (data not shown). These results suggest that, at least under this experimental setting, MMP-9 is the major MMP involved in the gelatinolysis in the tumor-bearing liver. The administration of catalase or Gal-CAT reduced the MMP-9 activity (lanes 4, for catalase, and 5, for Gal-CAT). More than 90% reduction was observed in the liver homogenates of the tumor-bearing mice treated with Gal-CAT.

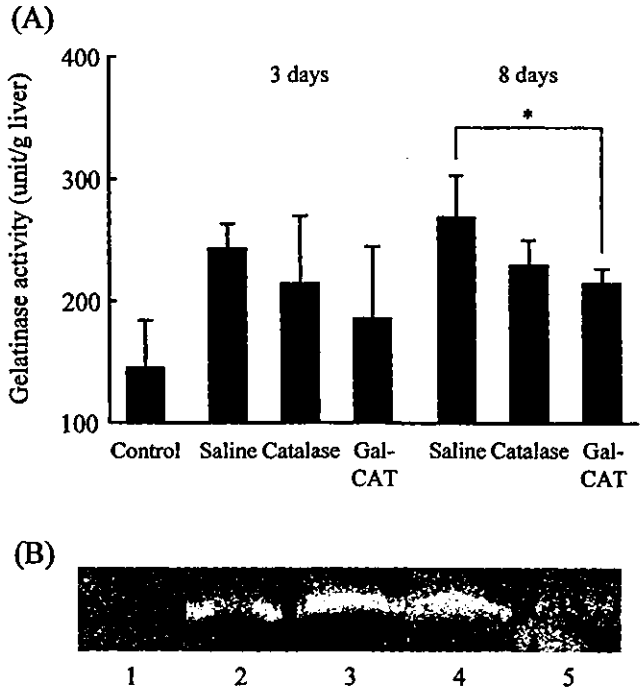

Figure 6. MMP activity in the liver of mice receiving intraportal injection of 1×10^5 colon 26 tumor cells followed by intravenous injection of saline, catalase or Gal-CAT. Each of catalase derivative was injected at a dose of 35 000 units/kg of body weight at 3 or 8 days after tumor inoculation. (A) Total MMP activity in liver homogenates was assayed. Results are expressed as the mean + SD of 4 mice.
*A statistically significant difference ($P < 0.05$). (B) MMP-9 activity in liver homogenates was visualized by gelatin zymography. Liver was sampled from control mice (lane 1), or from tumor-bearing mice treated at 8 days after tumor inoculation with saline (lanes 2 and 3), catalase (lane 4) or Gal-CAT (lane 5).

Discussion

It has been shown that ROS are involved in various aspects of tumor progression, invasion and metastasis and antioxidant enzymes alter those events by detoxifying their ligands. Two major groups of enzymes are frequently used for this purpose: catalase and SODs. However, the results obtained

so far with these enzymes vary from laboratory to laboratory depending on the enzymes and experimental systems used [17, 18, 30–34]. Although catalase and SOD are sometimes classified together as antioxidant enzymes, they should be separately considered because their reactions are completely different. SOD accelerates the dismutation rate of superoxide anion into H_2O_2 and oxygen, while catalase catabolizes H_2O_2 to water. We proposed the hypothesis that the elimination of H_2O_2 at the site where tumor metastasis occurs could reduce this event and, therefore, examined the action of the targeted delivery of catalase to liver tissue for inhibiting experimental liver metastasis of colon carcinoma cells.

In the animal model used in the present study, the colon carcinoma cells were injected intraportally to induce experimental hepatic metastasis. Therefore, the steps before adhesion to the target, i.e. tumor cell dissociation, invasion, and intravasation, are not included in the formation and inhibition of tumor metastasis in the present model. Then, the first step of the metastasis is the arrest of tumor cells in small vessels and adhesion to endothelial cells [1, 35]. The target organ for tumor metastasis depends greatly on the type of primary tumor, but the mechanism of organ-specific metastasis of tumor cells has not yet been fully clarified. Specific adhesion molecules on tumor cells and on vascular endothelial cells are suggested to be involved in determining the organ specificity of metastasis. Intraportal injection of colon 26 tumor cells resulted in the formation of a number of metastatic colonies on the surface of the liver (Figure 3), showing that some of the tumor cells injected survive, adhere to the endothelial cells, invade and proliferate. In contrast, when injected into a tail vein, the colon 26 tumor cells formed more than 90 metastatic colonies in the lung with few in the liver and spleen (less than 1 colony per organ) at 14 days after injection [27]. These results suggest that the initial step in the formation of metastasis of colon 26 tumor cells is mediated by physical trapping of the cells within the microvasculature in organs rather than by specific interaction between tumor cells and endothelial cells via adhesion molecules. The tissue distribution study supports the entrapment of the tumor cells within the liver following the injection of cells into the portal vein (Figure 2).

Hepatic sinusoidal cells play an important role in the early phase of hepatic metastasis. Depletion of Kupffer cell functions prior to tumor cell challenge increases metastatic growth in the liver [36, 37], indicating that these cells acts as a defense against liver metastasis. However, during the early period (1 h) following tumor cell infusion into a mesenteric vein, Bayon et al. [37] showed that the number of tumor cells entrapped in the liver was greater in Kupffer cell-free rats than in control animals. These results suggest that Kupffer cells can arrest tumor cells circulating within blood vessels and then kill them directly or by recruiting inflammatory cells. Therefore, activation of Kupffer cells can be one approach to inhibit tumor metastasis to the liver, although the ability of Kupffer cells to kill tumor cells is somewhat limited to a small number of tumor cells [38]. Recently, a similar role of natural killer cells to that of Kupffer cells in preventing liver metastasis has been reported [39]. The tumoricidal activity of sinusoidal cells, such as Kupffer cells, is mediated by several factors, including ROS [40]. Administration of antioxidant enzymes, therefore, might inhibit the initial tumoricidal activity of ROS produced by Kupffer cells. In the present study, we injected catalase derivatives into mice at three days after tumor injection, when Kupffer cells are thought to have little tumoricidal activity [37]. At three days, tumor cells are considered to be already adhering to endothelial cells and starting to extravasate and invade the tissue parenchyma of the liver. Although adhesion molecules and their ligands are known to play important roles in cell–cell or cell–ECM interactions and those levels are modified by ROS [26], the administration of catalase 3 days after the administration of colon 26 tumor cells will not affect their adhesion to sinusoidal endothelial cells. Possible metastatic processes affected by catalase are: extravasation, invasion, and proliferation, although these processes were not separately examined in the present study. The formation of metastatic colonies in the liver, the final result of these multi-step, complex processes, was assessed in relation to the elimination of H_2O_2 by targeted delivery of catalase.

MMPs are the main proteolytic enzymes involved in the invasion of tumor cells [41]. In the present model of metastatic tumors of colon 26 cells, a significant amount of gelatinase activity was detected in metastatic tumor-bearing mouse liver (Figure 5B). ECM and basement membranes act as physical barriers to tumor cells metastasizing from their original site to target organs. These barriers consist of various proteins such as collagens, fibronectin, and laminin. Of these proteins, type-IV collagen is very important because it constitutes the most rigid barrier to tumor metastasis. The ability of cancer cells to metastasize depends on the ability to degrade type-IV collagen. MMP-2 and -9 are well known as enzymes that can degrade type-IV collagen. The family of MMP have a zinc ion at the center of their active site, and more than 20 types of MMPs have discovered so far [41]. The expression of MMP-9 could be easily detected in the homogenates of tumor-bearing liver tissue in the present study (Figure 6B, lane 2). The treatment of mice receiving intraportal injection of colon 26 cells with Gal-CAT significantly reduced the total MMP activity in the liver homogenates (Figure 6A). These results are in good agreement with previous reports [5, 6] indicating that the MMP activity of the cells are, at least partially, regulated by the concentration of H_2O_2. In our preliminary study, the colon 26 tumor cells treated with H_2O_2 *in vitro* resulted in larger numbers of metastatic colonies in the lung following intravenous injection into mice [27]. Recently, Wenk et al. [42] have shown that H_2O_2 increases MMP-1 mRNA levels by using Mn-SOD-overexpressing fibroblasts. In addition, Nelson et al. [43] reported that elevated SOD activity increases MMP expression through augmenting H_2O_2 level in tumor cells. Therefore, in the hepatic metastatic model used in the current study, the suppression of MMP activity by detoxifying H_2O_2 would explain the inhibitory effect of catalase derivatives. The *in situ* zymography suggested that the gelatinase activities in the tumor-bearing liver were close to the sinusoids of the liver. The gelatin

zymographic analysis of liver homogenates clearly demonstrated that the MMP-9 is the major contributor in the gelatinolysis in the tumor-bearing mouse liver after intraportal inoculation of colon 26 tumor cells (Figure 6B). The MMP-9 activity, again, was drastically suppressed by an intravenous injection of Gal-CAT. No gelatinolytic bands were detected when (2R)-[(4-biphenylylsulfonyl)amino]-N-hydroxy-3-phenylpropionamide, which is reported to be a potent and highly selective inhibitor of MMP-9 and MMP-2 [44], was added to the polyacrylamide gel, supporting that the gelatinolytic activity was due to MMP-9. The interval between the administration of Gal-CAT and the sampling of the liver was as short as 18 h, and a doubling time of the tumor cells was more than 24 h in culture. Therefore, the number of the tumor cells in the liver of mice treated with Gal-CAT could be, at least, half or more in that treated with saline. Therefore, the great reduction in MMP activity suggests that not only the number of the tumor cells but also the generation or/and activation of MMP in the liver is suppressed by Gal-CAT. However, we cannot conclude which cells in the liver contribute to the gelatinase activities in the tumor-bearing liver. MMPs are known to be produced from various cells; they include tumor cells, endothelial cells, macrophages and hepatocytes [4–6, 45]. We confirmed that colon 26 tumor cells release MMPs in culture. Our preliminary results obtained using cultured hepatocytes and colon 26 tumor cells show that, under oxidative stress, MMP-9 is largely produced by hepatocytes, whereas MMP-2 is from colon 26 cells (Y. Kobayashi et al., unpublished data). These findings suggest that hepatocytes are the major source of the MMP detected in the liver containing metastatic tumor cells. Additional data are needed to identify the source of MMPs *in vivo*.

Even if catalase is involved in the inhibition of tumor metastasis by detoxifying H_2O_2, it might be effective only when reaches the sites where H_2O_2 is generated. In previous studies, we have shown that catalase can be delivered to hepatocytes or hepatic sinusoidal cells following chemical modification [24]. Unmodified bovine liver catalase is efficiently taken up by hepatocytes following intravenous injection into mice via an efficient, catalase-specific mechanism [20]. These biodistribution features would be an advantage for inhibiting liver metastasis. In an actual fact, an intravenous injection of catalase could reduce the number of metastatic colonies on the liver surface (Figure 3). Similar inhibitory effects of catalase on hepatic metastasis have been reported previously [17, 31].

Improvement of the inhibitory effect of catalase was investigated by altering its biodistribution characteristics by means of chemical modification. Galactosylation of catalase (Gal-CAT) increased the uptake rate by hepatocytes following intravenous injection [24] because it can be recognized by the asialoglycoprotein receptor that are only found on hepatocytes. On the other hand, Man-CAT and Suc-CAT were preferentially taken up by liver endothelial cells and Kupffer cells, via mannose receptors and scavenger receptors, respectively. These catalase derivatives preserve their enzymatic activity after modification and, in an ischemia/reperfusion hepatic injury model, Suc-CAT produced a better preventive effect than catalase [20, 26]. In the present study, however, Gal-CAT showed the highest inhibitory effect on the hepatic metastasis and the effects of Suc-CAT and Man-CAT were similar to that of catalase itself. These results suggest that the delivery of catalase to liver nonparenchymal cells is not effective as far as the prevention of tumor metastasis is concerned. It is difficult to conclude that the targeting of catalase to nonparenchymal cells, such as Kupffer cells, is as effective as delivery to hepatocytes, because a fraction of Suc-CAT and Man-CAT is delivered to hepatocytes via the catalase-specific mechanism. Although both catalase and Gal-CAT are predominantly taken up by hepatocytes after intravenous injection, the uptake rate is much greater for Gal-CAT than catalase [24]. An explanation is needed as to why the delivery of catalase via asialoglycoprotein receptor-mediated endocytosis is more effective than its delivery via the catalase-specific mechanism.

Hepatocytes contain a large quantity of catalase and the activity in the liver is about 84 000 ± 26 000 units/mouse liver, which is much greater than the injected dose of catalase derivatives (900 units/mouse). Most of the activity, however, localizes in the peroxisomes, and the catalase activity in the plasma is too low to be detected. Therefore, the injected catalase derivatives will exist in different locations from innate ones. If ROS are produced by the interaction between the tumor cells and hepatocytes, it is reasonable that the targeted delivery of catalase to hepatocytes by galactosylation is effective in reducing the number of metastatic colonies in the liver, even though catalase is not delivered directly to the tumor cells. It is reported that hepatocytes are the major source of MMP-9 in cytokine-activated hepatocytes and in regenerating livers after partial hepatectomy [45]. Therefore, hepatocytes may be the right target of catalase delivery for the inhibition of hepatic tumor metastasis, and the superior effect of Gal-CAT would support this hypothesis. Catalase derivatives targeted to several cell-surface receptors such as Gal-CAT, Man-CAT and Suc-CAT hardly dissociate from receptors after binding but internalized. Therefore, we think that there is little chance for the targeted catalase to be delivered to other cells after binding to the receptors. Further studies are needed to understand the underlying mechanisms of the inhibition by catalase delivery.

In conclusion, targeted delivery of catalase to hepatocytes via the asialoglycoprotein receptor can markedly suppress the formation of colonies in the liver following intraportal injection of colon carcinoma cells. Detoxification of H_2O_2 decreased the MMP activity in the liver containing metastatic tumor tissues that would be involved in the inhibitory effects of catalase derivatives. These findings indicate that hepatocyte-directed delivery of catalase is an efficient approach to preventing hepatic metastasis.

Acknowledgements

This work was supported in part by grants-in-aid for Scientific Research from the Ministry of Education, Science,

Sports, and Culture of Japan and by grants from the Ministry of Health, Labour and Welfare of Japan.

References

1. Engers R, Gabbert HE. Mechanisms of tumor metastasis: Cell biological aspects and clinical implications. J Cancer Res Clin Oncol 2000; 126: 682–92.
2. Onoda JM, Piechocki MP, Honn KV. Radiation-induced increase in expression of the αIIbβ3 integrin in melanoma cells: Effects on metastatic potential. Radiat Res 1992; 130: 281–8.
3. Sellak H, Franzini E, Hakim J et al. Reactive oxygen species rapidly increase endothelial ICAM-1 ability to bind neutrophils without detectable upregulation. Blood 1994; 83: 2669–77.
4. Shaughnessy SG, Whaley M, Lafrenie RM et al. Walker 256 tumor cell degradation of extracellular matrices involves a latent gelatinase activated by reactive oxygen species. Arch Biochem Biophys 1993; 304: 314–21.
5. Rajagopalan S, Meng XP, Ramasamy S et al. Reactive oxygen species produced by macrophage-derived foam cells regulate the activity of vascular matrix metalloproteinases *in vitro*. Implications for atherosclerotic plaque stability. J Clin Invest 1996; 98: 2572–9.
6. Belkhiri A, Richards C, Whaley M et al. Increased expression of activated matrix metalloproteinase-2 by human endothelial cells after sublethal H_2O_2 exposure. Lab Invest 1997; 77: 533–9.
7. Mukai M, Shinkai K, Tateishi R et al. Macrophage potentiation of invasive capacity of rat ascites hepatoma cells. Cancer Res 1987; 47: 2167–71.
8. Murrell GA, Francis MJ, Bromley L. Modulation of fibroblast proliferation by oxygen free radicals. Biochem J 1990; 265: 659–65.
9. Adamson IY, Young L, Orr FW. Tumor metastasis after hyperoxic injury and repair of the pulmonary endothelium. Lab Invest 1987; 57: 71–7.
10. Szatrowski TP, Nathan CF. Production of large amounts of hydrogen peroxide by human tumor cells. Cancer Res 1991; 51: 794–8.
11. Ben-Yoseph O, Ross BD. Oxidation therapy: The use of a reactive oxygen species-generating enzyme system for tumour treatment. Br J Cancer 1994; 70: 1131–5.
12. Fang J, Sawa T, Akaike T et al. Tumor-targeted delivery of polyethylene glycol-conjugated D-amino acid oxidase for antitumor therapy via enzymatic generation of hydrogen peroxide. Cancer Res 2002; 62: 3138–43.
13. Jessup JM, Battle P, Waller H et al. Reactive nitrogen and oxygen radicals formed during hepatic ischemia-reperfusion kill weakly metastatic colorectal cancer cells. Cancer Res 1999; 59: 1825–9.
14. Mavier P, Guigui B, Preaux AM et al. *In vitro* toxicity of hydrogen peroxide against normal vs. tumor rat hepatocytes: Role of catalase and of the glutathione redox cycle. Hepatology 1988; 8: 1673–8.
15. Van Driel BE, Van Noorden CJ. Oxygen insensitivity of the histochemical assay of glucose-6-phosphate dehydrogenase activity for the discrimination between nonmalignant and malignant cells. J Histochem Cytochem 1999; 47: 575–82.
16. Malafa M, Margenthaler J, Webb B et al. MnSOD expression is increased in metastatic gastric cancer. J Surg Res 2000; 88: 130–134.
17. Nonaka Y, Iwagaki H, Kimura T et al. Effect of reactive oxygen intermediates on the *in vitro* invasive capacity of tumor cells and liver metastasis in mice. Int J Cancer 1993; 54: 983–6.
18. Yoshizaki N, Mogi Y, Muramatsu H et al. Suppressive effect of recombinant human Cu, Zn-superoxide dismutase on lung metastasis of murine tumor cells. Int J Cancer 1994; 57: 287–92.
19. Fujita T, Nishikawa M, Tamaki C et al. Targeted delivery of human recombinant superoxide dismutase by chemical modification with mono- and polysaccharide derivatives. J Pharmacol Exp Ther 1992; 263: 971–8.
20. Yabe Y, Koyama Y, Nishikawa M et al. Hepatocyte-specific distribution of catalase and its inhibitory effect on hepatic ischemia/reperfusion injury in mice. Free Radic Res 1999; 30: 265–74.
21. Nishikawa M, Ohtsubo Y, Ohno J et al. Pharmacokinetics of receptor-mediated hepatic uptake of glycosylated albumin in mice. Int J Pharm 1992; 85: 75–85.
22. Takakura Y, Fujita T, Furitsu H et al. Pharmacokinetics of succinylated proteins and dextran sulfate in mice: Implications for hepatic targeting of protein drugs by direct succinylation via scavenger receptors. Int J Pharm 1994; 105: 19–29.
23. Fujita T, Furitsu H, Nishikawa M et al. Therapeutic effects of superoxide dismutase derivatives modified with mono- or polysaccharides on hepatic injury induced by ischemia/reperfusion. Biochem Biophys Res Commun 1992; 189: 191–6.
24. Yabe Y, Nishikawa M, Tamada A et al. Targeted delivery and improved therapeutic potential of catalase by chemical modification: combination with superoxide dismutase derivatives. J Pharmacol Exp Ther 1999; 289: 1176–84.
25. Mihara K, Oka Y, Sawai K et al. Improvement of therapeutic effect of human recombinant superoxide dismutase on ischemic acute renal failure in the rat via cationization and conjugation with polyethylene glycol. J Drug Target 1994; 2: 317–21.
26. Yabe Y, Kobayashi N, Nishihashi T et al. Prevention of neutrophil-mediated hepatic ischemia/reperfusion injury by SOD and catalase derivatives. J Pharmacol Exp Ther 2001; 298: 894–9.
27. Nishikawa M, Tamada A, Kumai H et al. Inhibition of experimental pulmonary metastasis by controlling biodistribution of catalase in mice. Int J Cancer 2002; 99: 474–9.
28. Miyahara T, Samejima T. Effects of halide ions on porcine kidney catalase. J Biochem 1982; 91: 525–35.
29. Thakur ML, Coleman RE, Welch MJ. Indium-111-labeled leukocytes for the localization of abscesses: Preparation, analysis, tissue distribution, and comparison with gallium-67 citrate in dogs. J Lab Clin Med 1977; 89: 217–28.
30. Safford SE, Oberley TD, Urano M et al. Suppression of fibrosarcoma metastasis by elevated expression of manganese superoxide dismutase. Cancer Res 1994; 54: 4261–5.
31. Anasagasti MJ, Alvarez A, Martin JJ et al. Sinusoidal endothelium release of hydrogen peroxide enhances very late antigen-4-mediated melanoma cell adherence and tumor cytotoxicity during interleukin-1 promotion of hepatic melanoma metastasis in mice. Hepatology 1997; 25: 840–6.
32. Kogawa K, Muramatsu H, Tanaka M et al. Enhanced inhibition of experimental metastasis by the combination chemotherapy of Cu-Zn SOD and adriamycin. Clin Exp Metast 1999; 17: 239–44.
33. Tanaka M, Kogawa K, Nishihori Y et al. Suppression of intracellular Cu-Zn SOD results in enhanced motility and metastasis of Meth A sarcoma cells. Int J Cancer 1997; 73: 187–92.
34. Takenaga M, Igarashi R, Ochiai A, Mizushima Y. Effect of lecithinized superoxide dismutase (PC-SOD) on experimental pulmonary metastasis in mice. Free Radic Biol Med 1999; 26: 1117–25.
35. Blood CH, Zetter BR. Tumor interactions with the vasculature: Angiogenesis and tumor metastasis. Biochim Biophys Acta 1990; 1032: 89–118.
36. Pearson HJ, Anderson J, Chamberlain J et al. The effect of Kupffer cell stimulation or depression on the development of liver metastases in the rat. Cancer Immunol Immunother 1986; 23: 214–6.
37. Bayon LG, Izquierdo MA, Sirovich I et al. Role of Kupffer cells in arresting circulating tumor cells and controlling metastatic growth in the liver. Hepatology 1996; 23: 1224–31.
38. Phillips NC. Kupffer cells and liver metastasis. Optimization and limitation of activation of tumoricidal activity. Cancer Metast Rev 1989; 8: 231–52.
39. Rushfeldt C, Sveinbjornsson B, Seljelid R et al. Early events of hepatic metastasis formation in mice: Role of Kupffer and NK-cells in natural and interferon-gamma-stimulated defense. J Surg Res 1999; 82: 209–15.
40. Nathan CF. Secretory products of macrophages. J Clin Invest 1987; 79: 319–26.
41. Curran S, Murray GI. Matrix metalloproteinases: Molecular aspects of their roles in tumour invasion and metastasis. Eur J Cancer 2000; 36: 1621–30.
42. Wenk J, Brenneisen P, Wlaschek M et al. Stable overexpression of manganese superoxide dismutase in mitochondria identifies hydrogen peroxide as a major oxidant in the AP-1-mediated induction of matrix-degrading metalloprotease-1. J Biol Chem 1999; 274: 25869–76.
43. Nelson KK, Ranganathan AC, Mansouri J et al. Elevated sod2 activity augments matrix metalloproteinase expression: Evidence for the in-

volvement of endogenous hydrogen peroxide in regulating metastasis. Clin Cancer Res 2003; 9: 424–32.

44. Tamura Y, Watanabe F, Nakatani T et al. Highly selective and orally active inhibitors of type IV collagenase (MMP-9 and MMP-2): N-sulfonylamino acid derivatives. J Med Chem. 1998; 41: 640–9.

45. Haruyama T, Ajioka I, Akaike T et al. Regulation and significance of hepatocyte-derived matrix metalloproteinases in liver remodeling. Biochem Biophys Res Commun 2000; 272: 681–6.

Physicochemical, Tissue Distribution, and Vasodilation Characteristics of Nitrosated Serum Albumin: Delivery of Nitric Oxide *In Vivo*

HIDEMASA KATSUMI,[1] MAKIYA NISHIKAWA,[2] SHEN-FENG MA,[1] FUMIYOSHI YAMASHITA,[1] MITSURU HASHIDA[1]

[1]Departments of Drug Delivery Research. Graduate School of Pharmaceutical Sciences, Kyoto University, Sakyo-ku, Kyoto 606-8501, Japan

[2]Biopharmaceutics and Drug Metabolism, Graduate School of Pharmaceutical Sciences, Kyoto University, Sakyo-ku, Kyoto 606-8501, Japan

Received 2 February 2004; revised 30 April 2004; accepted 4 May 2004

Published online 2 July 2004 in Wiley InterScience (www.interscience.wiley.com). DOI 10.1002/jps.20147

ABSTRACT: Conjugates of nitric oxide (NO) to serum albumins are candidates for controlled delivery of NO *in vivo*, but their physicochemical and tissue distribution characteristics have hardly been examined yet. In this study, to achieve its *in vivo* delivery, bovine serum albumin (BSA) was reacted with sodium nitrite to obtain NO-BSA, which had 0.25–0.28 molecules of S-nitrosothiol/BSA. In addition to cystein, other amino acid residues were modified by the reaction. The conjugation had no significant effect on the molecular weight, but reduced the electric charge and induced reversible changes in the secondary structure of BSA. After intravenous injection in mice at a dose of 1 mg/kg, ^{111}In-NO-BSA slowly disappeared from plasma in a similar manner to ^{111}In-BSA, but showed greater accumulation in the liver and kidney. NO-BSA induced a transient decrease in arterial pressure after intravenous injection in rats at a dose of 100 mg/kg, and significantly increased the distribution of ^{111}In-BSA to the lung in mice. These results indicate that NO is released from NO-BSA shortly after injection, and this NO decreases blood pressure and increases the distribution of macromolecules to the lung. These findings provide useful basic information for designing macromolecular NO donors able to achieve controlled delivery of NO. J Pharm Sci 93:2343–2352, 2004

Keywords: conjugation; distribution; macromolecular drug delivery; pharamcokinetics; albumin

INTRODUCTION

Nitric oxide (NO) is involved in a wide variety of physiological and pathological processes. They include vascular smooth muscle relaxation,[1–3] inhibition of platelet aggregation,[4,5] neurotransmission,[6] and immune regulation.[7–9] Because NO elicits protective and beneficial actions in various disease states, NO delivery is expected to be effective in the treatments for essential hypertension, stroke, coronary artery disease, vascular complications of diabetes, erectile dysfunction, and other disorders involving the vascular system.[10] Vasodilation induced by NO would also be useful for improving the permeability of macromolecules across the vascular endothelium, which may solve the delivery problems of associated with genes and proteins.[11]

On the other hand, NO is reported to be cytotoxic in some situations.[12] NO degrades iron-containing prosthetic groups resulting in the inhibition of the mitochondrial respiratory chain and DNA synthesis.[13] NO also reacts with the superoxide anion that is produced by activated

Correspondence to: Mitsuru Hashida (Telephone: +81-75-753-4525; Fax: +81-75-753-4575; E-mail: hashidam@pharm.kyoto-u.ac.jp)

Journal of Pharmaceutical Sciences, Vol. 93, 2343–2352 (2004)

macrophages and other cells, to form peroxynitrite. Its protonated form acts as a potent chemical oxidant,[13] which induces modification of protein functions and DNA damage.[14]

These pieces of evidence suggest that the tissue distribution of NO needs to be well controlled to obtain the therapeutic benefits of NO. Because NO has a very short half life (~0.1 s) *in vivo*,[15] NO donors that generate NO after administration have been developed and used for NO delivery. However, little attention has been paid to the tissue distribution, or controlled delivery of NO *in vivo*. Of the various strategies possible, conjugation of NO to macromolecules appears to be a good approach to control the delivery of NO, because the tissue distribution of the macromolecules can be controlled by various techniques of chemical modification.[16] So far, conjugation of NO to serum albumin or other proteins has been reported,[17,18] and NO-conjugated serum albumin exhibits a number of biological activities of NO such as vasodilation and the inhibition of platelet aggregation. However, their pharmacokinetic properties have been hardly examined so far. It is well known that various kinds of chemically modified proteins are rapidly cleared by scavenging systems in the liver and spleen.[19,20] To control the delivery of NO, the effects of conjugation of NO to the carrier molecule on the tissue distribution of the NO-carrier conjugate should be examined.

In the present study, therefore, we selected bovine serum albumin (BSA, molecular weight of 67,000) as a macromolecular carrier of NO, because serum albumin is an endogenous carrier of NO,[15] and its tissue distribution characteristics are well known. To provide basic information for controlled delivery of NO *in vivo*, we synthesized NO-conjugated BSA (NO-BSA) with various degrees of modification, and analyzed the physicochemical characteristics of NO-BSA such as the apparent molecular weight, electric charge, and the structural characteristics, all of which are determinants of tissue distribution. Then, we examined the tissue distribution of NO-BSA after intravenous injection in mice. Finally, the vasodilating effects of NO-BSA were evaluated in mice and rats after intravenous injection of NO-BSA.

MATERIALS AND METHODS

Animals

Male ddY mice (25–27 g) and male Wistar rats (240–260 g) were purchased from the Shizuoka Agricultural Cooperative Association for Laboratory Animals (Shizuoka, Japan). Animals were maintained under conventional housing conditions. All animal experiments were conducted in accordance with the principles and procedures outlined in the National Institute of Health Guide for the Care and Use of Laboratory Animals. The protocols for animal experiments were approved by the Animal Experimentation Committee of the Graduate School of Pharmaceutical Sciences of Kyoto University.

Chemicals

BSA, sodium nitrite, sulfanilamide and *N*-(1-naphthyl)ethylenediamine dihydrochloride were purchased from Sigma Chemical (St. Louis, MO). Pharmalyte TM 2.5–5 for IEF was purchased from Amersham (Buckinghamshire, England). Amberlyte IRN-150L was purchased from Pharmacia biotech (Uppsala, Sweden). [^{111}In]Indium chloride was supplied by Nihon Medi-Physics (Takarazuka, Japan). Ammonium sulfamate and $HgCl_2$ were purchased from Wako Chemical (Osaka, Japan). All other chemicals were obtained commercially as reagent-grade products.

Synthesis of NO-BSA

NO-BSA with various degrees of modification was synthesized by reacting different amounts of sodium nitrite with BSA as reported previously.[17,18] In brief, BSA (50 mg) and a 200-, 500-, 1000-fold molar excess sodium nitrite was dissolved in 0.5 M HCl. The mixture was stirred for 15 min at 37°C and the reaction terminated by neutralizing the solution at pH 7.5 by the addition of 1 M NaOH and 0.5 M Tris buffer. The products were dialyzed against ultrapure water and concentrated by ultrafiltration at 4°C. UV-visible spectroscopy of NO-BSA was performed with a Beckman spectrometer at a concentration of 2 mg/mL NO-BSA in 0.1 M phosphate buffer at pH 7.4, 25°C. Products were coded as NO(200)-, NO(500)-, and NO(1000)-BSA, according to the molar ratio of sodium nitrite and BSA in the reaction mixture.

Number of NO Adducts on NO-BSA

The number of NO adducts on NO-BSA was determined by Saville assay.[21] In brief, a solution of NO-BSA was mixed with 0.5% ammonium sulfamate in 0.4 M HCl (total volume of 80 μL) for

1 min to remove existing NO_2 and HNO_2 from the solution. Eighty microliters 0.4 M HCl solution containing 3% sulfanilamide and 0.25% $HgCl_2$ was added, followed by the addition of 80 μL 0.1% *N*-(1-naphthyl)ethylenediamine dihydrochloride in 0.4 M HCl. To determine the number of S-nitrosothiol groups on NO-BSA, the mixture was incubated at room temperature for 10 min and the absorbance was read at 540 nm. Separately, to determine the number of total NO adducts on NO-BSA, the mixture was incubated for 5 h at room temperature. The number of NO adducts on NO-BSA was calculated according to a standard curve prepared with 2.5–100 μM $NaNO_2$. The number of free amino groups was determined by trinitrobenzene sulfonic acid using glycine as a standard.[22]

Molecular Weight and Isoelectric Point of NO-BSA

The apparent molecular weight of NO-BSA was estimated by nonreducing SDS-PAGE at 4°C using a standard curve prepared with a set of marker proteins (full range rainbow marker, Amersham, Buckinghamshire, England). The isoelectric point of NO-BSA was determined by isoelectric focusing (NA-1410, Nihon Eidou, Tokyo, Japan) under acidic conditions at 4°C. The gel was composed of acrylamide, bisacrylamide, glycerol, pharmalyte TM 2.5–5 for IEF, amberlyte IRN-150L, TEMED, and ammonium persulfate, and 0.1 M H_2SO_4 and 0.1 M NaOH were used as an anolyte and catholyte, respectively. Samples were applied to the cathode side and subjected to electrophoresis at 100 V for 30 min, 200 V for 30 min, and 400 V for 2 h. The Isoelectric Focusing Calibration Kit (Amersham, Buckinghamshire, England) was used as isoelectric point markers. These assays were performed at 4°C, because NO-BSA is more stable in the solution at low temperature.[17]

Tryptophanyl Fluorescence Spectrum

Intrinsic fluorescence spectra of BSA and NO-BSA were obtained on a RF-540 spectrofluorophotometer (Shimazu, Kyoto, Japan) at 25°C, with a 1-cm quartz cell, thermostatically controlled devices and 10-nm excitation and 5-nm emission bandwidths. BSA and NO-BSA were excited at 295 nm, and the spectra were corrected for buffer baseline fluorescence.

Circular Dichroism (CD) Spectrum

CD spectra of BSA and NO-BSA were measured using a JASCO J-820-type spectropolarimeter (JASCO, Tokyo, Japan) at 25°C. For calculation of the mean residue ellipticity [θ], the molecular weight of BSA and NO-BSA was taken as 67,000. Far-UV and near-UV CD spectra were recorded at protein concentrations of 5 and 15 μM, respectively, in 20 mM sodium phosphate buffer (pH 7.4).

Radiolabeling of BSA and NO-BSA

For the tissue distribution experiments, BSA and NO-BSA were radiolabeled with ^{111}In using the bifunctional chelating agent DTPA anhydride according to the method of Hnatowich et al.[23] In brief, each sample (5 mg) was dissolved in 1 mL 0.1 M HEPES buffer, pH 7, and mixed with two- or threefold molar DTPA anhydride in 10 μL dimethyl sulfoxide. The mixture was stirred for 15 min at room temperature, and the radiolabeled product was purified by gel filtration at 4°C using a Sephadex G-25 column (Pharmacia) to remove unreacted DTPA. The fractions containing the sample were collected and concentrated by ultrafiltration at 4°C. Then, 20 μL $^{111}InCl_3$ solution (37 MBq/mL) was added to 20 μL of 0.1 M citrate buffer, pH 5.5, and 40 μL DTPA-coupled derivative solution was added to the mixture. After 15 min, the mixture was applied to a PD-10 column and eluted with 0.1 M citrate buffer, pH 5.5. The derivative fractions were collected and concentrated by ultrafiltration at 4°C. Radiochemical purity of ^{111}In-BSA and ^{111}In-NO-BSA was confirmed by cellulose acetate electrophoresis, which was run at an electrostatic field of 0.8 mA/cm for 30 min in veronal buffer ($I = 0.06$, pH 8.6). The presence of NO on NO-BSA after radiolabeling was confirmed by the Saville assay as described above.

Tissue Distribution Experiment

Each ^{111}In-NO-BSA was injected into the tail vein of mice at a dose of 1 mg/kg. At appropriate times after injection, blood was collected from the vena cava under ether anesthesia, and the mice were then killed. Heparin sulfate was used as an anticoagulant. Plasma was obtained from the blood by centrifugation. The muscle, liver, kidney, spleen, heart, and lung were removed, rinsed with saline,

and weighed. Urine was also collected. The radioactivity in each sample was counted using a well-type NaI-scintillation counter (ARC-500, Aloka, Tokyo, Japan).

Calculation of Pharmacokinetic Parameter

The ^{111}In radioactivity concentrations in plasma were normalized with respect to the % of the dose/mL and analyzed using the nonlinear least-squares program MULTI.[24] The tissue distribution profiles were evaluated using tissue uptake clearance (CL_{tissue}) according to integration plot analysis. By dividing the amount in a tissue at time t (X_t) and the area under the plasma concentration-time curve (AUC) from time 0 to t (AUC_{0-t}) by the plasma concentration at time t (C_t), CL_{tissue} was obtained from the slope of the plot of X_t/C_t versus AUC_{0-t}/C_t.

Blood Pressure after Intravenous Injection of NO-BSA into Rats

Blood pressure was measured by a strain gauge pressure transducer (P10EZ, Viggo-Spectramed Japan Co., Ltd., Tokyo, Japan) connected to a catheter inserted into the femoral artery of rats. Systolic blood pressure (SBP) and diastolic blood pressure (DBP) before and after the injection of NO(1000)-BSA were recorded every 30 s with a polygraph (poly-Graph 366 system, NEC San-ei Instruments, Co., Ltd., Corporation, Tokyo, Japan), connected to a microcomputer (Dyna-Book J-3100SS, Toshiba Corporation, Tokyo, Japan). NO(1000)-BSA was given by intravenous injection at a dose of 100 mg/kg. Mean arterial blood pressure (MAP) was calculated from SBP and DBP using the following equation:

$$MAP(mmHg) = (SBP\text{-}DBP)/3 + DBP$$

Effect of NO-BSA on Tissue Distribution of BSA in Mice

The effects of NO-BSA on vascular permeability of macromolecules were evaluated as reported previously [25] with some slight modification. Briefly, ^{111}In-BSA was injected into the tail vein of mice at a dose of 1 mg/kg. At 10 min after injection, NO(1000)-BSA or BSA was injected into the tail vein at a dose of 100 mg/kg. NO(1000)-BSA preincubated for 3 h at 37°C was also used as a control. At 1 min and 5 min after the injection of NO(1000)-BSA or BSA, the blood was collected from the vena cava, then the mice were killed by bleeding. Collecting blood was started at about 5 s before the time indicated, because collecting sufficient volume of blood for analysis takes about 10 s. Then, several tissue samples were collected. The flux of ^{111}In-BSA to tissue was calculated as:

$$\text{Flux} = N/C_P$$

where N is the amount of ^{111}In- BSA in a tissue (expressed as cpm/g tissue) and C_P is the concentration of ^{111}In-BSA in plasma (expressed as cpm/mL blood) at each time point.

RESULTS

Synthesis and Characterization of NO-BSA

The reaction of BSA with sodium nitrite under an acidic conditions produced yellowish solutions with an absorption maximum at 330–350 nm, which is a characteristic of nitrosation products. An absorption peak at 540–545nm, a marker of S-nitrosothiol, was also detected (data not shown). These spectroscopic data were similar to those reported previously.[18]

The number of NO adducts and modified amino groups, apparent molecular weight, and isoelectric point of NO-BSA are summarized in Table 1. The

Table 1. Physicochemical Characteristics of NO-BSA

Compound	Total NO/BSA[a] (mol/mol)	S-NO/BSA[a] (mol/mol)	Molecular Weight[b]	Number of Modified Amino Groups[c] (mol/mol)	Isoelectric Point
BSA	0	0	67,000	0	4.8
NO(200)-BSA	0.70	0.23	67,000	13.4	4.7–4.8
NO(500)-BSA	0.76	0.21	67,000	18.4	4.6–4.7
NO(1000)-BSA	0.79	0.19	67,000	20.5	4.5–4.6

[a]The total NO adducts and S-NO adducts on BSA were estimated by the Saville assay.
[b]The molecular weights of compounds were estimated by nonreducing SDS-PAGE.
[c]The number of modified amino groups were determined by the TNBS method.

total number of NO adducts increased on increasing the concentration of sodium nitrite in the reaction mixture from 0.70 to 0.79. However, the number of S-nitrosothiol groups decreased on increasing in the concentration from 0.23 to 0.19, probably due to the oxidation of thiol.[18,26] Before nitrosation, BSA had 0.38 mol of free SH/mol of protein as determined by the Ellman assay (data not shown), which was consistent with results reported in a previous report.[26] Nitrosation did not significantly alter the apparent molecular weight of any preparation of NO-BSA, whereas the isoelectric point was reduced depending on the degree of chemical modification. The number of modified amino groups increased on increasing the concentration of sodium nitrite from 13 to 21.

Tryptophanyl Fluorescence Spectrum

BSA has two tryptophan residues, one of them being located in an aqueous solvent-exposed environment.[27] We measured the tryptophanyl fluorescence to examine whether the tryptophan residues are nitrosated. As seen in Figure 1, any preparation of NO-BSA had a lower relative fluorescence intensity than BSA. In addition, the λ_{max} was also slightly blue-shifted from 346 to 342 nm. After a 3-h incubation of NO-BSA at 37°C, the fluorescence spectrum of NO-BSA tended to return to that of BSA. These results suggest the possibility that NO bound to the tryptophan residue on BSA is released by incubation, and the structural change produced by modification near the residue is reversible.

CD Spectrum

The secondary structure of BSA and NO-BSA was analyzed by measuring the far-UV CD. The CD spectra of NO(1000)-BSA was slightly shifted compared with that of BSA (Fig. 2). In addition, the near-UV CD spectra of NO(1000)-BSA was also slightly shifted (data not shown). After a 3-h incubation of NO(1000)-BSA at 37°C, both the far-UV and near-UV CD spectra of NO(1000)-BSA became closer to those of BSA.

Distribution of ^{111}In-NO-BSA after Intravenous Injection in Mice

Figure 3 shows the time courses of the concentrations in plasma and the liver and kidney concentrations of ^{111}In-radioactivity after intravenous injection of ^{111}In-BSA or ^{111}In-NO-BSA in mice at a dose of 1 mg/kg. As reported previously, ^{111}In-BSA slowly disappeared from the blood circulation. ^{111}In-NO(200)-BSA, ^{111}In-NO(500)-BSA, and ^{111}In-NO(1000)-BSA also slowly disappeared from the blood circulation in a similar manner to ^{111}In-BSA. However, all ^{111}In-NO-BSAs showed greater accumulation in the liver and kidney during the first hour after injection; the amounts of radioactivity recovered in the liver were 0.6 ±

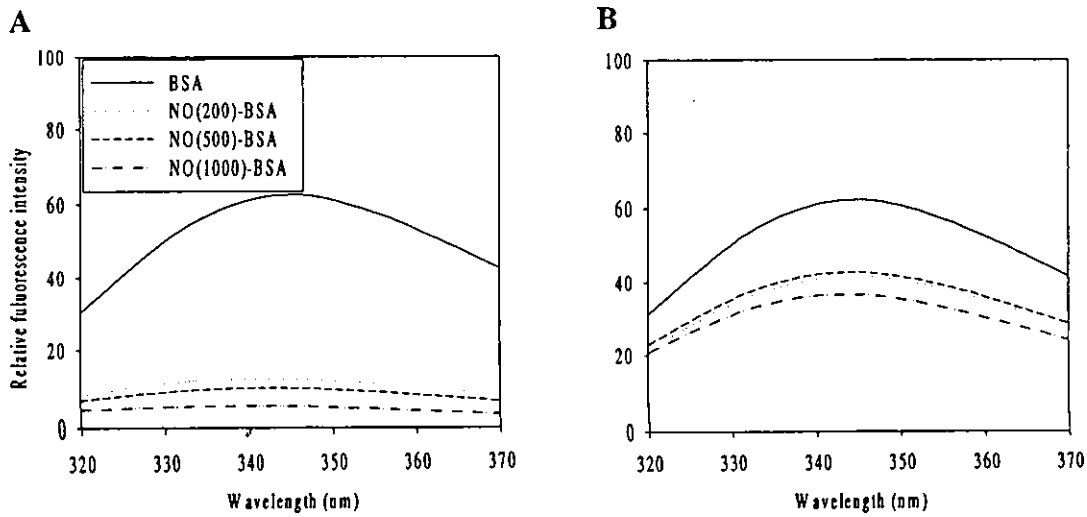

Figure 1. Intrinsic fluorescence spectra of BSA and NO-BSA at 25°C. Each sample solution (2 μM in 0.1 M sodium phosphate buffer, pH 7.4) was excited at 295 nm and the emission fluorescence was detected from 320 to 370 nm. (A) protein without incubation; (B) protein incubated for 3 h at 37°C.

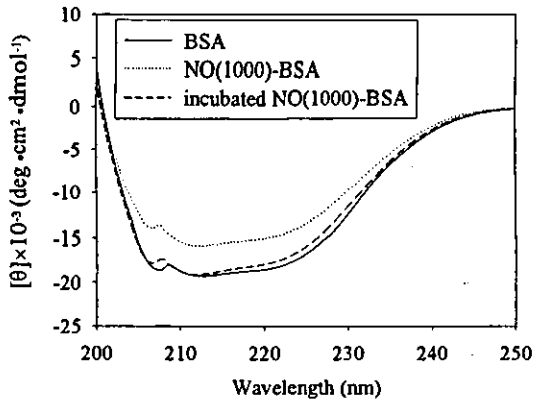

Figure 2. Far-UV CD spectra of BSA and NO-BSA at 25°C. The protein concentration was set at 5 μM in 20 mM sodium phosphate buffer (pH 7.4).

0.6, 4.7 ± 0.7, 4.9 ± 0.9, and 12.1 ± 1.5% of the dose for ^{111}In-BSA, ^{111}In-NO(200)-BSA, ^{111}In-NO-(500), and ^{111}In-NO(1000)-BSA, respectively. Thereafter, however, any ^{111}In-NO-BSA showed no significant accumulation in those organs.

Calculation of AUC and Clearance

For a quantitative comparison of the distribution profiles between BSA and NO-BSA, the total body (CL_{total}), liver (CL_{liver}), and kidney (CL_{kidney}) clearances, as well as the AUC, were calculated based on the distribution data (Table 2). The CL_{total} of ^{111}In-NO-BSA was proportional to the degree of modification, and CL_{kidney} and CL_{liver} accounted for most of the CL_{total}. CL_{kidney} and CL_{liver} calculated for the first 1 h after injection were greater than those at later times, suggesting that the uptake of NO-BSA by these organs is faster at early period of time.

Blood Pressure of Rats after Intravenous Injection of NO-BSA

Figure 4 shows the mean arterial blood pressure (MAP) of rats after intravenous injection of NO(1000)-BSA at a dose of 100 mg/kg. NO(1000)-BSA induced a transient decrease in MAP im-

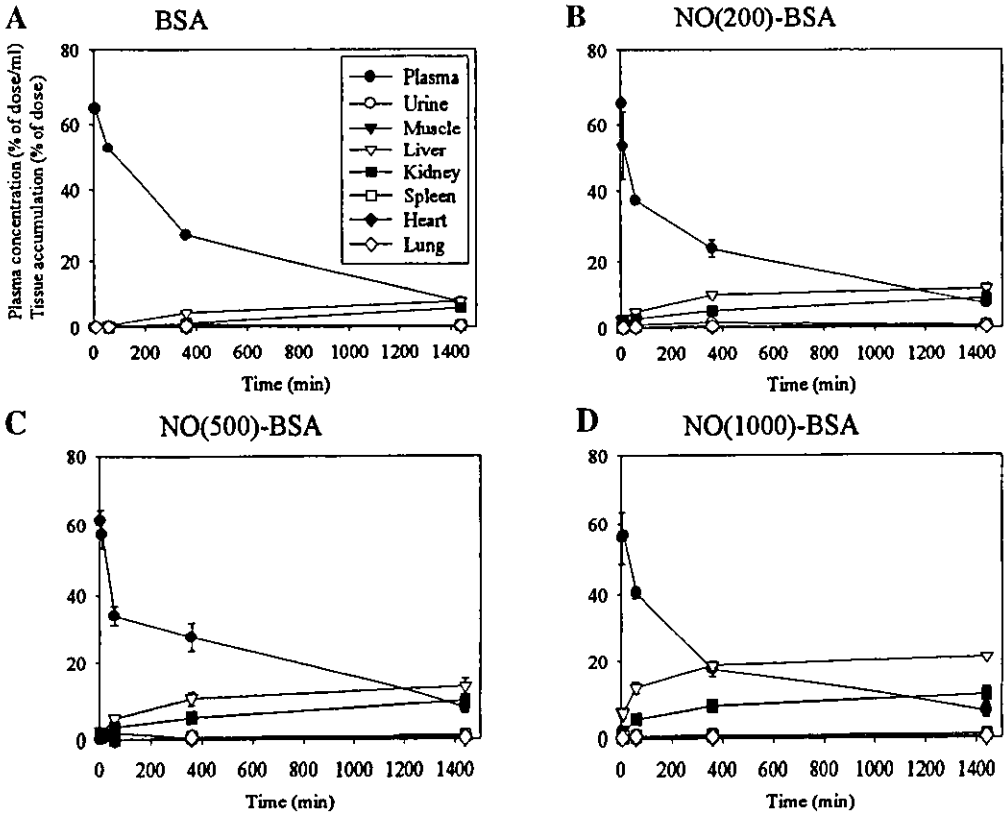

Figure 3. Time-courses of plasma concentration and tissue accumulation of ^{111}In-BSA (A), ^{111}In-NO(200)-BSA (B), ^{111}In-NO(500)-BSA, (C) and ^{111}In-NO(1000)-BSA (D) in mice after intravenous injection of a dose of 1 mg/kg. ●, plasma; ○, urine; ▼, muscle; ▽, liver; ■, kidney; □, spleen; ◆, heart; ◇, lung. The results are expressed as mean ± SD of three mice.

Table 2. AUC and Clearances of ^{111}In-BSA and ^{111}In-NO-BSA after Intravenous Injection in Mice at a Dose of 1 mg/kg

Compound	AUC (% of Dose (h/mL)	Total Body Clearance (μL/h)	Hepatic Clearance (μL/h)		Renal Clearance (μL/h)	
			0–1 h	1–24 h	0–1 h	1–24 h
BSA	588	154	7.0	13.3	11.5	9.7
NO(200)-BSA	501	157	70.8	22.8	43.7	18.2
NO(500)-BSA	426	166	72.8	28.2	47.1	20.8
NO(1000)-BSA	439	193	240	30.7	91.7	15.7

mediately after intravenous injection. BSA had no significant effects on the blood pressure (data not shown). The fall in pressure was transient and there was a return to the initial levels in 3 min.

Effect of NO-BSA on Tissue Distribution of ^{111}In-BSA

Figure 5 shows the effects of NO-BSA on the tissue distribution of ^{111}In-BSA. NO(1000)-BSA significantly ($p < 0.05$) increased the ^{111}In-BSA flux of the lung at 1 min after injection. However, the flux of other organs exhibited no significant changes. An injection of NO(1000)-BSA preincubated at 37°C for 3 h had no significant effect on the distribution of ^{111}In-BSA (data not shown).

DISCUSSION

Although acidified NO_2^- can react with several functional groups on proteins, only two kinds of amino acid residues, cystein and tryptophan, were found to be nitrosated in a previous study.[26] We also determined the nitrosated cystein residue by UV-visible spectroscopy and the Saville assay, and showed the possibility of nitrosated tryptophan residue from the fluorescence spectrum. Other amino acid residues, such as arginine, lysine, asparagine, glutamine, and tyrosine, may have undergone initial nitrosation to some extent. However, nitrosation of the primary amine group in arginine, lysine, asparagine, and glutamine resulted in unstable products that decomposed via diazotization and denitrogenation. Nitrosation of tyrosine is followed by irreversible oxidation of –NO to $-NO_2$.[28,29] Among these residues, we clearly demonstrated that the primary amine of lysine residues was modified. The number of the modified amino groups increased on increasing the concentration of sodium nitrite.

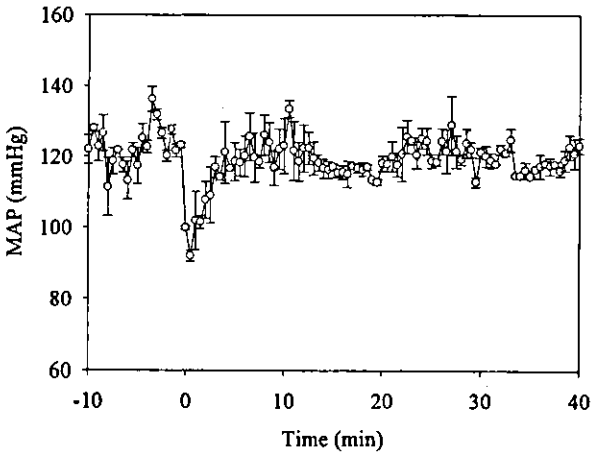

Figure 4. Blood pressure of rats after intravenous injection of NO(1000)-BSA at a dose of 100 mg/kg. ○, MAP (mean arterial blood pressure). Results are expressed as mean ± SD of three rats.

It has been shown that several chemically modified proteins are vulnerable to capture by mononuclear phagocytes. Therefore, protein derivatives with a strong negative charge, such as succinylated or acconitylated proteins, are delivered to the liver, spleen, and kidney after intravenous injection.[19,20,30–33] The hepatic and renal uptake of ^{111}In-aconitylated BSA is dependent on the strength of the overall negative charge of the derivatives.[33] As demonstrated in these previous studies, the physicochemical characteristics such as electric charge and molecular weight play an important role in the tissue distribution of protein derivatives. In the present study, nitrosation hardly altered the apparent molecular weight of BSA but slightly increased the negative charge. These results can be explained by the facts that NO or NO derivatives are small molecules and the lysine residues are modified. The electric charge and number of modified amino groups of NO-BSA did not return to the original value after a 3-h incubation at 37°C.

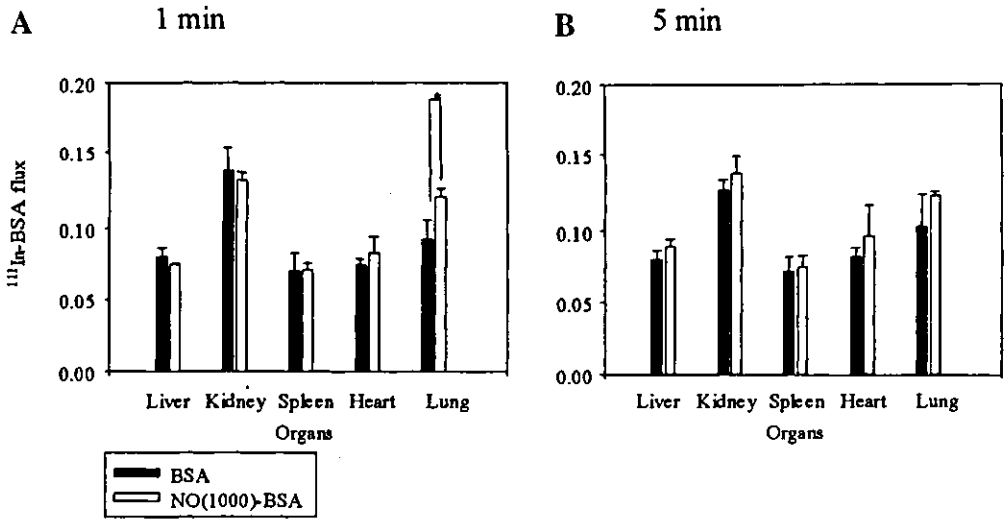

Figure 5. Changes in ^{111}In-BSA flux in various organs at 1 min (A) and 5 min (B) after intravenous injection of BSA, NO(1000)-BSA at a dose of 100 mg/kg into mice. Results are expressed as mean ± SD of three mice. Statistically significant difference was assessed using Student's *t*-test ($^*p < 0.05$).

The overall structure of the protein is also important for its tissue distribution. Based on the spectra data, the structure of NO-BSA was somewhat altered by nitrosation. Such alterations detected in the spectra, however, seemed to be reversible because a 3-h incubation at 37°C almost completely abolished the differences in the spectra between BSA and NO-BSA. The reversion in the structural characteristics of NO-BSA following incubation are related to the release of NO from NO-BSA, which was detected both in buffer and in plasma by the Griess method (data not shown).

^{111}In-NO-BSA showed a little initial uptake by the liver and kidney after intravenous injection. These distribution results suggest that the hepatic and renal distribution of NO-BSA is due to both the increased negative charge and the alteration in the structure of BSA. However, CL_{kidney} and CL_{liver} calculated at later times after injection were lower than those for the first hour. This is probably due to the reversion in the structural characteristics of NO-BSA by the release of NO from NO-BSA with time, which is supported by the CD spectra of NO-BSA. In the case of succinylation, 28 or more lysine residues of BSA needed to be modified for rapid uptake by the liver and kidney, and a derivative with 20 modified lysine residues showed less, but significant accumulation in these organs.[20] Thirty-two or more lysine residues of BSA were needed to be modified with aconityl anhydride for remarkable changes in the electric charge in our previous study.[33] The number of modified lysine residues on NO-BSA was 21 or less in the present study, so the change in the electric charge could have a little effect on the tissue distribution of NO-BSA. However, our data indicate the importance of the reaction condition for synthesizing NO-BSA, because the number of modified lysine residues increases on increasing in the concentration of sodium nitrite. A further increase in the concentration may result in additional modification on lysine residues, leading to rapid uptake of NO-BSA by the liver and kidney. The dose used in the tissue distribution study was adjusted to 1 mg/kg, which is much lower than that used in the experiments for blood pressure measurement (100 mg/kg), because the tissue uptake of chemically modified proteins is generally prominent at lower doses. In our previous study, succinylated BSA showed an extensive hepatic uptake at doses of 1 mg/kg or smaller, but the uptake decreased with an increasing dose.[20] Because NO-BSA showed little tissue uptake even at the low dose of 1 mg/kg, it would slowly disappear from the blood circulation when injected at 100 mg/kg. NO was completely released from NO-BSA in at least 5 min after intravenous injection, as detected by measuring nitrite in plasma by the Griess method (data not shown). This rapid release explains the transient decrease in MAP after its administration to rats. No significant change in MAP by BSA supports the possibility that the released NO from NO-BSA reduces the blood pressure in rats. The release of NO from NO-protein has been reported to be ac-

celerated in the presence of low molecular weight thiols such as gulutathione and a trace amount of copper ion.[34] Therefore, the half-life of NO release from NO-BSA in vivo should be very short, because both components are present in the blood. On the other hand, it is very stable in solutions containing no such components at room temperature. Stamler et al. reported that the half-life of NO-BSA in phosphate buffer (pH7.4, 25°C) was ~24 h.[17] In our preliminary experiments, the release of NO from NO-BSA was much slower than that of SNAP or S-nitrosoglutathion in phosphate buffer solution containing 10% serum at 37°C in the dark, as detected by measuring nitrite in solution by the Griess method.

^{111}In-BSA flux of the lung increased significantly following an intravenous injection of NO-BSA. These results, together with those on the blood pressure, indicate that NO is rapidly released from NO-BSA after injection, and the NO released exhibits its pharmacological activities. The endothelial permeability of the serum proteins is related to the number and distribution of the capillaries, and blood content of tissues.[35] Because the lung has a continuous endothelium, it is not clear whether BSA can pass through the vascular endothelium in the lung after injection of NO-BSA.

Based on the results, we conclude that serum albumin is a promising molecule as NO carrier *in vivo*. Similar to most NO donors, however, NO-BSA needs to be further modulated to control the release of NO to achieve long-term delivery of therapeutic concentrations of NO. Increasing the number of NO would be another major challenge for developing more effective NO delivery systems. The findings of this study provide useful basic information for designing macromolecular NO donors able to achieve controlled delivery of NO.

ACKNOWLEDGMENTS

The authors are grateful to Dr. T. Mukai, Kyoto University, for helpful advice on the radiolabeling of NO-BSA and to Dr. M. Kakemi, Osaka University of Pharmaceutical Sciences, for supporting measurement of blood pressure.

REFERENCES

1. Ignarro LJ. 1989. Heme-dependent activation of soluble guanylate cyclase by nitric oxide: Regulation of enzyme activity by porphyrins and metalloporphyrins. Semin Hematol 26:63–76.
2. Ignarro LJ. 1989. Endothelium-derived nitric-oxide—Pharmacology and relationship to the actions of organic nitrate esters. Pharmacol Res 6:651–659.
3. Moncada S, Palmer RMJ, Gryglewski RJ. 1986. Mechanism of action of some inhibitors of endothelium-derived relaxing factor. Proc Natl Acad Sci USA 83:9164–9168.
4. Azuma H, Ishikawa M, Sekizaki S. 1986. Endothelium-dependent inhibition of platelet aggregation. Br J Pharmacol 88:411–415.
5. Furlong B, Henderson AH, Lewis MJ, Smith JA. 1987. Endothelium-derived relaxing factor inhibits *in vitro* platelet aggregation. Br J Pharmacol 90: 687–692.
6. Garthwaite J. 1991. Glutamate, nitric oxide and cell–cell signaling in the nervous system. Trends Neurosci 14:60–67.
7. Hibbs JB. 1991. Synthesis of nitric oxide from L-arginine—A recently discovered pathway induced by cytokines with antitumor and antimicrobial activity. Res Immunol 142:565–569.
8. Marletta MA, Yoon PS, Iyengar R, Leaf CD, Wishnok JS. 1988. Macrophage oxidation of L-arginine to nitrite and nitrate—Nitric oxide is an intermediate. Biochemistry 27:8706–8711.
9. Stuehr DJ, Gross SS, Sakuma I, Levin R, Nathan CF. 1989. Activated murine macrophages secrete a metabolite of arginine with the bioactivity of endothelium-derived relaxing factor and the chemical-reactivity of nitric oxide. J Exp Med 169:1011–1020.
10. Ignarro LJ. 2002. Wei Lun Visiting Professorial Lecture: Nitric oxide in the regulation of vascular function: An historical overview. J Card Surg 17: 301–306.
11. Nishikawa M, Huang L. 2001. Nonviral vectors in the new millennium: Delivery barriers in gene transfer. Hum Gene Ther 12:861–870.
12. Laval F, Wink DA. 1994. Inhibition by nitric oxide of the repair protein, O6-methylguanine-DNA-methyltransferase. Carcinogenesis 15:443–447.
13. Hibbs JB Jr, Taintor RR, Vavrin Z, Rachlin EM. 1988. Nitric oxide: A cytotoxic activated macrophage effector molecule. Biochem Biophys Res Commun 157:87–94.
14. Beckman JS, Crow JP. 1993. Pathological implications of nitric oxide, superoxide and peroxynitrite formation. Biochem Soc Trans 21:330–334.
15. Kelm M, Schrader J. 1990. Control of coronary vascular tone by nitric oxide. Circ Res 66:1561–1575.
16. Takakura Y, Hashida M. 1996. Macromolecular carrier systems for targeted drug delivery: Pharmacokinetic considerations on biodistribution. Pharm Res 13:820–831.

17. Stamler JS, Simon DI, Osborne JA, Mullins ME, Jaraki O, Michel T, Singel DJ, Loscalzo J. 1992. S-nitrosylation of proteins with nitric oxide: synthesis and characterization of biologically active compounds. Proc Natl Acad Sci USA 89:444–448.
18. Simon DI, Mullins ME, Jia L, Gaston B, Singel DJ, Stamler JS. 1996. Polynitrosylated proteins: Characterization, bioactivity, and functional consequences. Proc Natl Acad Sci USA 93:4736–4741.
19. Jansen RW, Olinga P, Harms G, Meijer DK. 1993. Pharmacokinetic analysis and cellular distribution of the anti-HIV compound succinylated human serum albumin (Suc-HSA) in vivo and in the isolated perfused rat liver. Pharm Res 10:1611–1614.
20. Yamasaki Y, Sumimoto K, Nishikawa M, Yamashita F, Yamaoka K, Hashida M, Takakura Y. 2002. Pharmacokinetic analysis of in vivo disposition of succinylated proteins targeted to liver nonparenchymal cells via scavenger receptors: importance of molecular size and negative charge density for in vivo recognition by receptors. J Pharmacol Exp Ther 301:467–477.
21. Saville B. 1958. A scheme for the colorimetric determination of microgram amounts of thiols. Analyst 83:670–672.
22. Habeeb AF. 1966. Determination of free amino groups in proteins by trinitrobenzenesulfonic acid. Anal Biochem 14:328–336.
23. Hnatowich DJ, Layne WW, Childs RL. 1982. The preparation and labeling of DTPA-coupled albumin. Int J Appl Radiat Isot 33:327–332.
24. Yamaoka K, Tanigawara Y, Nakagawa T, Uno T. 1981. A pharmacokinetic analysis program (multi) for microcomputer. J Pharmacobiodyn 4:879–885.
25. Singh S, Anning PB, Winlove CP, Evans TW. 2001. Regional transcapillary albumin exchange in rodent endotoxaemia: Effects of fluid resuscitation and inhibition of nitric oxide synthase. Clin Sci (Lond) 100:81–89.
26. Zhang YY, Xu AM, Nomen M, Walsh M, Keaney JF Jr, Loscalzo J. 1996. Nitrosation of tryptophan residue(s) in serum albumin and model dipeptides. Biochemical characterization and bioactivity. J Biol Chem 271:14271–14279.
27. Peters T Jr. 1985. Serum albumin. Adv Protein Chem 37:161–245.
28. Challis BC. 1989. Chemistry and biology of nitrosated peptides. Cancer Surv 8:363–384.
29. Bonnett R, Nicolaidou P. 1977. Nitrite and the environment. The nitrosation of α-amino acid derivatives. Heterocycles 7:637–659.
30. Takakura Y, Fujita T, Furitsu H, Nishikawa M, Sezaki H, Hashida M. 1994. Pharmacokinetics of succinylated proteins and dextran sulfate in mice: Implications for hepatic targeting of protein drugs by direct succinylation via scavenger receptors. Int J Pharm 105:19–29.
31. Furitsu H, Ogawara K, Fujita T, Yamashita F, Takakura Y, Sezaki H, Hashida M. 1997. Pharmacokinetic analysis of scavenger receptor-mediated uptake of anionized proteins in the isolated rat liver. Int J Pharm 151:15–26.
32. Kuipers ME, Swart PJ, Schutten M, Smit C, Proost JH, Osterhaus AD, Meijer DK. 1997. Pharmacokinetics and anti-HIV-1 efficacy of negatively charged human serum albumins in mice. Antiviral Res 33:99–108.
33. Yamasaki Y, Hisazumi J, Yamaoka K, Takakura Y. 2003. Efficient scavenger receptor-mediated hepatic targeting of proteins by introduction of negative charges on the proteins by aconitylation: The influence of charge density and size of the proteins molecules. Eur J Pharm Sci 18:305–312.
34. Singh RJ, Hogg N, Joseph J, Kalyanaraman B. 1996. Mechanism of nitric oxide release from S-nitrosothiols. J Biol Chem 271:18596–18603.
35. Deng X, Wang X, Andersson R. 1995. Endothelial barrier resistance in multiple organs after septic and nonseptic challenges in the rat. J Appl Physiol 78:2052–2061.

Available online at www.sciencedirect.com
SCIENCE DIRECT®
ELSEVIER
Vaccine 22 (2004) 2609–2616
Vaccine
www.elsevier.com/locate/vaccine

Induction of cytotoxic T lymphocytes following immunization with cationized soluble antigen

Tomoko Ikenaga, Yasuomi Yamasaki, Kohsuke Shakushiro, Makiya Nishikawa, Yoshinobu Takakura*

Department of Biopharmaceutics and Drug Metabolism, Graduate School of Pharmaceutical Sciences, Kyoto University, Sakyo-ku, Kyoto 606-8501, Japan

Received 22 September 2003; received in revised form 28 November 2003; accepted 11 December 2003
Available online 30 January 2004

Abstract

Antigen presentation on major histocompatibility complex (MHC) class I and subsequent priming of antigen-specific cytotoxic T lymphocytes (CTLs) are essential steps for vaccination but exogenous soluble proteins are conventionally taken up by endosomes and presented on MHC class II rather than class I. In this study, we demonstrated, for the first time, that ovalbumin (OVA) chemically cationized with hexamethylenediamine (HMD) can induce OVA-specific CTLs without any adjuvants. Cationization of OVA greatly enhances cellular uptake by antigen-presenting cells (APCs) through adsorptive endocytosis. Two kinds of Cat-OVAs with different cationic charges were evaluated to elicit a CTL response through enhanced uptake by APCs and concomitant participation in the class I pathway. Cat_{20}-OVA, a cationized OVA derivative with more cationic charges, showed pronounced induction of the OVA-specific CTL response after subcutaneous immunization. The CTL response was comparable with that induced by OVA with CFA. In contrast to the CFA formulation that actually produced local tissue damage in this study, local damage at the injection sites was not observed with Cat-OVAs. Cat_{20}-OVA also showed a significant protective effect on the growth of OVA-expressing E.G7 tumor cells. In conclusion, cationization of soluble antigen is a useful and safe vaccination strategy.

Keywords: CTLs; Cationization; Soluble antigen

1. Introduction

In vaccination aimed at the treatment of cancer or infectious diseases, antigen presentation on major histocompatibility complex (MHC) class I and subsequent priming of antigen-specific cytotoxic T lymphocytes (CTLs) are essential steps. However, exogenous antigen proteins administered as vaccines are conventionally taken up by endosomes and presented on MHC class II rather than class I [1]. On the other hand, it is well-known that the process, cross-presentation, in which exogenous antigens are presented on MHC class I appears when a large quantity of antigen is taken up by antigen-presenting cells (APCs) through phagocytosis [2,3], macropinocytosis [4], or receptor-mediated endocytosis [5–7]. Hence, the failure to prime antigen-specific CTLs may be partly attributed to inadequate delivery of antigens to APCs. Among APCs, dendritic cells (DCs) play an important role in inducing cellular immunity because of their unique ability to cross-prime $CD8^+$ T cells more effectively than any other APCs [5,8] and to stimulate naive T cells [9] followed by generating a CTL response. Therefore, an approach delivering large quantity of antigens to DCs is desirable for efficient induction of antigen-specific CTLs. Soluble proteins without adjuvants would be useful and safe vaccines if they could produce antigen-specific CTL efficiently.

Cationic proteins are efficiently taken up by cells through adsorptive endocytosis based on electrostatic interaction because the surface of the cell membrane has negative charges [10–14]. Chemical modification of antigen proteins to introduce a positive charge is expected to enhance cellular uptake. Although adsorptive endocytosis is a non-specific process, catioinized antigen proteins would be taken up by cells including APCs in vivo following local injection and consequently may induce an antigen-specific CTL response.

In this study, we used ovalbumin (OVA) as a model antigen and synthesized cationized OVA derivatives with different cationic charges. Here we have demonstrated that the soluble cationized OVA can be efficiently presented on MHC class I in vitro and elicit antigen-specific CTLs in vivo.

* Corresponding author. Tel.: +81-75-753-4615; fax: +81-75-753-4614.
E-mail address: takakura@pharm.kyoto-u.ac.jp (Y. Takakura).

0264-410X/$ – see front matter © 2003 Elsevier Ltd. All rights reserved.
doi:10.1016/j.vaccine.2003.12.023

2. Materials and methods

2.1. Chemicals

Ovalbumin, hexamethylenediamine (HMD), 1-ethyl,3-(3-dimethylaminopropyl)-carbodiimide (EDAC) and fluorescein isothiocyanate (FITC) were purchased from Sigma (St. Louis, MO). Diethylenetriaminepentaacetic acid (DTPA) anhydride was purchased from Dojindo Laboratory (Kumamoto, Japan). OVA peptide, SIINFEKL was purchased from Bachem (Budendorf, Switzerland). $^{111}InCl_3$ was supplied by Nihon Medi-Physics (Takarazuka, Japan). $Na_2{}^{51}CrO_4$ was purchased from Daiichi Radioisotope Laboratories (Tokyo, Japan). All other chemicals were reagent-grade products obtained commercially.

2.2. Cells and animals

DC2.4 cells, a cell line of murine dendritic cells (haplotype H-2^b) [3], were kindly provided by Dr. K.L. Rock (University of Massachusetts Medical School, Worcester, MA). CD8OVA1.3 cells, T hybridoma cells against SIINFEKL-K^b [15], were a generous gift from Dr. C.V. Harding (Case Western Reserve University, Cleveland, OH). EL4 cells, C57BL/6 T lymphoma, and E.G7 cells, OVA-transfected clone of EL4 [16], were purchased from American Type Culture Collection (Manassas, VA).

DC2.4 was cultured in RPMI 1640 medium (Nissui Pharmaceuticals, Tokyo, Japan) supplemented with 10% heat-inactivated fetal bovine serum (Equitech-Bio, Kerrville, TX), 50 μM 2-mercaptoethanol, 2 mM L-glutamine, and antibiotics (all from Invitrogen, Carlsbad, CA). CD8OVA1.3 and EL4 were cultured in Dulbecco's modified Eagle medium (Nissui) supplemented as described for RPMI 1640 medium. E.G7 was cultured in RPMI 1640 medium supplemented with 10% heat-inactivated fetal bovine serum, 50 μM 2-mercaptoethanol, 2 mM L-glutamine, glucose, sodium pyruvate, HEPES and G418.

Five-week-old male ddY mice and 6-week-old female C57BL/6 mice were purchased from the Shizuoka Agricultural Cooperative Association for Laboratory Animals (Shizuoka, Japan). Animals were maintained under conventional housing conditions.

2.3. Cationization of OVA

OVA was dissolved in HMD and the pH was adjusted to 5.5 with HCl the water was added to give a total volume of 4.3 ml. After stirring on ice for 40 min, EDAC was added and then the mixture was continuously stirred for 1 h at room temperature (RT). Then the same amount of EDAC was added and reacted for 5 h at RT. The product was dialyzed through membrane (MWCO: 3500) at 4 °C to remove free reactant followed by ultrafiltration and lyophilization. The degree of cationization was assessed by estimating the additional amino groups as measured by trinitrobenzensulfonic acid (TNBS) [17]. The synthesis conditions of Cat-OVAs and physico-chemical characteristics of native OVA and Cat-OVAs are shown in Table 1.

Table 1
Synthesis condition and physico-chemical characteristics of native OVA and Cat-OVAs

	Amount of reactant used in modification			Modified carboxyl groups	Net charge
	OVA (mg)	HMD (μl)	EDAC (mg)		
OVA				0	−5
Cat_9-OVA	80	400	25 × 2	8.53	+12
Cat_{20}-OVA	100	800	53 × 2	20.3	+36

2.4. Internalization and visualization of native OVA and Cat-OVAs

OVA and Cat-OVAs were labeled with FITC by the method of Monsigny et al. [18]. About (1–2) × 10^5 per well DC2.4 was seeded on glass coverslips in 12-well plates. After complete adhesion, the cells were washed with phosphate-buffered saline (PBS) and incubated at 37 °C, in 5% CO_2 for 1 h with FITC-labeled OVA (1 mg/ml) or Cat-OVAs (200 μg/ml) dissolved in 1 ml Hanks' balanced salt solution (HBSS). After incubation, the protein solution was removed, and the cells were washed three times with ice-cold PBS, followed by fixing with 4% parafolmaldehyde in PBS, and incubating at RT for more than 20 min. After washing twice with PBS, they made permeable and the nuclei were stained as described previously [19]. In brief, they were treated with 0.2% Triton X-100–PBS for permealization, 15 μg/ml RNase A and 0.5 μg/ml propidium iodide in 0.1 M Tris–HCl (pH 7.4) containing 0.1 M NaCl. Then they were mounted in glycerol:PBS (1:1) containing 2.5% 1,4-diazobicyclo(2,2,2)octane. Images were obtained by confocal laser scanning microscopy (MRC-1024, Bio-Rad, Hercules, CA).

2.5. Antigen presentation assay

Various concentrations of antigen proteins were applied to DC2.4 (5 × 10^4 per well) cultured on a 96-well plate and incubated with CD8OVA1.3 (1 × 10^5 per well) for 24 h in 5% CO_2 at 37 °C. After the cells were centrifuged (1500 rpm) for 5 min, the supernatants were harvested and freeze thawed. Then the response of CD8OVA1.3 was determined by measuring IL-2 levels in the supernatants with ELISA (OptEIA™ Mouse IL-2 Set and TMB Substrate Reagent Set, Pharmingen, San Diego, CA).

2.6. In vitro cytotoxicity assay

Cytotoxicity was evaluated by MTT assay that was previously described [20]. After DC2.4 were coincubated with